

Full Length Article

Development and characterization of a novel RE³⁺ doped Core-shell CeO₂ abrasive system and its glass CMP investigations

Zhuolun Li^a, Liangmao Jin^b, Zhiqiang Cao^b, Chong Zhang^c, Xin Cao^c, Gaorong Han^a, Shou Peng^c, Yong Liu^{a,*}

^a School of Materials Science and Engineering, Zhejiang University, Hangzhou 310027, China

^b Bengbu China Optoelectronics Technology Co., Ltd., No.199, Shiwu Road, Bengbu City, Anhui Province, China

^c CNBM Research Institute for Advanced Glass Materials Group Co., Ltd., No.1047, Tushan Road, Bengbu City, Anhui Province, China

ARTICLE INFO

Keywords:
PS@CeO₂
Chemical Mechanical Polish (CMP)
Glass Polish

ABSTRACT

In recent years, Ultra-Thin Glass (UTG) has attracted substantial market attention due to its multi-scenario applications. One of the technical cores in UTG manufacturing is the abrasive design of the chemical mechanical polishing (CMP) process. The present work proposed rare-earth-doped core-shell structured PS@CeO₂, PS@CeO₂:La, and PS@CeO₂:Yb abrasives synthesized by a low-temperature two-step method. The core-shell abrasives are large uniform nanospheres with a size of about 375 nm ~ 450 nm. According to the matching effect of RE³⁺ radii and defect sizes, La³⁺ with larger radii exhibits a more substantial modulation effect than Yb³⁺ upon the lattice distortion and Ce³⁺/Ce⁴⁺ chemical shift. The CMP results revealed the superior polishing efficiency and better flattening ability of core-shell abrasives. The optimized PS@CeO₂:La shows the best glass polishing ability ($MRR = 480.22 \text{ nm/min}$, $R_a = 0.32 \text{ nm}$), which is attributed to the increased Ce³⁺ composition from 9.79% to 28.14% (compared with the pristine PS@CeO₂) and large particle size, indicative of potential applications of novel abrasive systems in the field of glass polishing.

1. Introduction

With the rapid advancement of communication technology, the screen display system has been updated and iterated in the direction of ultra-thin and flexible in recent years [1]. For its high chemical stability, low product costs, and tolerance to heat treatment, Ultra-Thin Glass (UTG) has substantial market potential and scientific research values in many fields, such as flexible OLEDs [2], wearable electrochemical sensors [3], micro-fluidic chips [4], and foldable displays [5]. Even several technologies, including overflow down-draw, slit pull-down, and float processes, could fabricate glass sheets allowing the minimum thickness to be a few micrometers, the glass substrates still need to be polished to achieve efficient thinning and a precisely flat surface, which is still very challenging now.

Because of the high planarization ability and precise controllability for specific applications, chemical mechanical polishing (CMP) is critical in many fabrications requiring flat and smooth surfaces, such as ultra-precision optical components [6], ultra-large-scale integrated circuit devices [7], and liquid crystal glass substrates [8]. In a typical CMP

process, material removal and flattening are achieved by the synergistic effect of abrasive mechanical friction and chemical corrosion [9]. Compared to conventional abrasives, like SiO₂ [10–11] and Al₂O₃ [12], CeO₂ with oxygen vacancies and unique Ce³⁺/Ce⁴⁺ redox pair contributes significantly to the chemical corrosion function on glass material removal [9], exhibiting high polishing efficiency and is considered as one of the most promising CMP abrasives.

The polishing characteristics of the CeO₂-based abrasives are highly dependent on the size [13], shape [14], and mixture [15] at the nanoscale. Oh et al. reported that the oxide CMP removal rate monotonously increases with the particle size of CeO₂ abrasives [13]. However, the size distribution and morphology of conventional ceria abrasives are challenging to be controlled with calcination, and scratches or other mechanical damages may occur during material removal processes. Recently, the core-shell structured composites were introduced into CMP, due to their round surface morphology, narrow size distribution, and low elastic moduli [16–18], which could effectively decrease scratch defects [19]. The PS core size [20] and CeO₂ shell thickness [21] have been found that significantly affect the CMP performance due to

* Corresponding author at: School of Materials Science and Engineering, Zhejiang University, Hangzhou 310027, PR China.
E-mail address: liuyong.mse@zju.edu.cn (Y. Liu).

Table 1
Polishing parameters.

Parameter	Specifications
Head rotating speed	100 rpm
Pad rotating speed	150 rpm (same direction as the head)
Slurry flow rate	31 ml/min
Polishing pressure	5 N (1.81 psi)
Polishing time	1.5 min

Table 2
Nominal and Measured Doping concentration, the average particle size of the synthesized core–shell CeO₂-based abrasives.

Samples	Doping concentration (%)		Average particle size (nm)	
	Nominal	Measured by ICP	statistics by SEM	test by light scattering
PS@CeO ₂	–	–	377	375
PS@CeO ₂ : La	4.4	4.41	381	386
PS@CeO ₂ : Yb	4.4	4.43	392	396

the spring-like effect. However, most of the research on CMP applies to integrated circuits, and research on the polishing ability of PS@CeO₂ is conducted on silicon wafers, with insufficient research on its polishing performance on glass surfaces.

On the other hand, the chemical-tooth effect, the solid-state tribological reaction between CeO₂ abrasives and the substrate surface

[22], plays a vital role in CMP, and it has been proposed that Ce³⁺ in CeO₂, instead of Ce⁴⁺, assists in breaking Si-O bond during CMP. Thus many studies devoted to enriching the Ce³⁺ concentration in CeO₂ by decreasing particle size [23], calcination with hydrogen [24], lowering the CeO₂ content in polishing slurry [25], and introducing dopants.

In the present work, a novel abrasive system that applies the combination of chemical modification that regulates the chemical activity of CeO₂ via doping rare earth ions and structure optimization via establishing the core–shell structure was conducted, which was facilely achieved by a low-temperature wet chemistry method. Moreover, the CMP performance of the novel lanthanide doping core–shell PS@CeO₂ abrasive on the glass is first investigated and thoroughly compared with that of the available CeO₂ abrasives bought from the market. The results indicate that core–shell abrasives are large uniform nanospheres, and the doping rare earth ions (La³⁺ and Yb³⁺) effectively regulate the crystalline structure and chemical shift of Ce³⁺/Ce⁴⁺, which benefit the glass polish efficiency. The optimal abrasive, La³⁺ doped PS@CeO₂, significantly improves the polishing material removal rate by 42.07%, compared with the commercial abrasives. The relevance of rare earth ion doping, CeO₂ microscopic phases, and glass polishing performance have been discussed in detail.

2. Experimental details

2.1. Materials

Absolute ethanol (C₂H₅OH, ≥99.5%), sodium hydroxide (NaOH, ≥96.0%), potassium persulfate (KPS, ≥99.5%), methyl acrylic acid (AA,

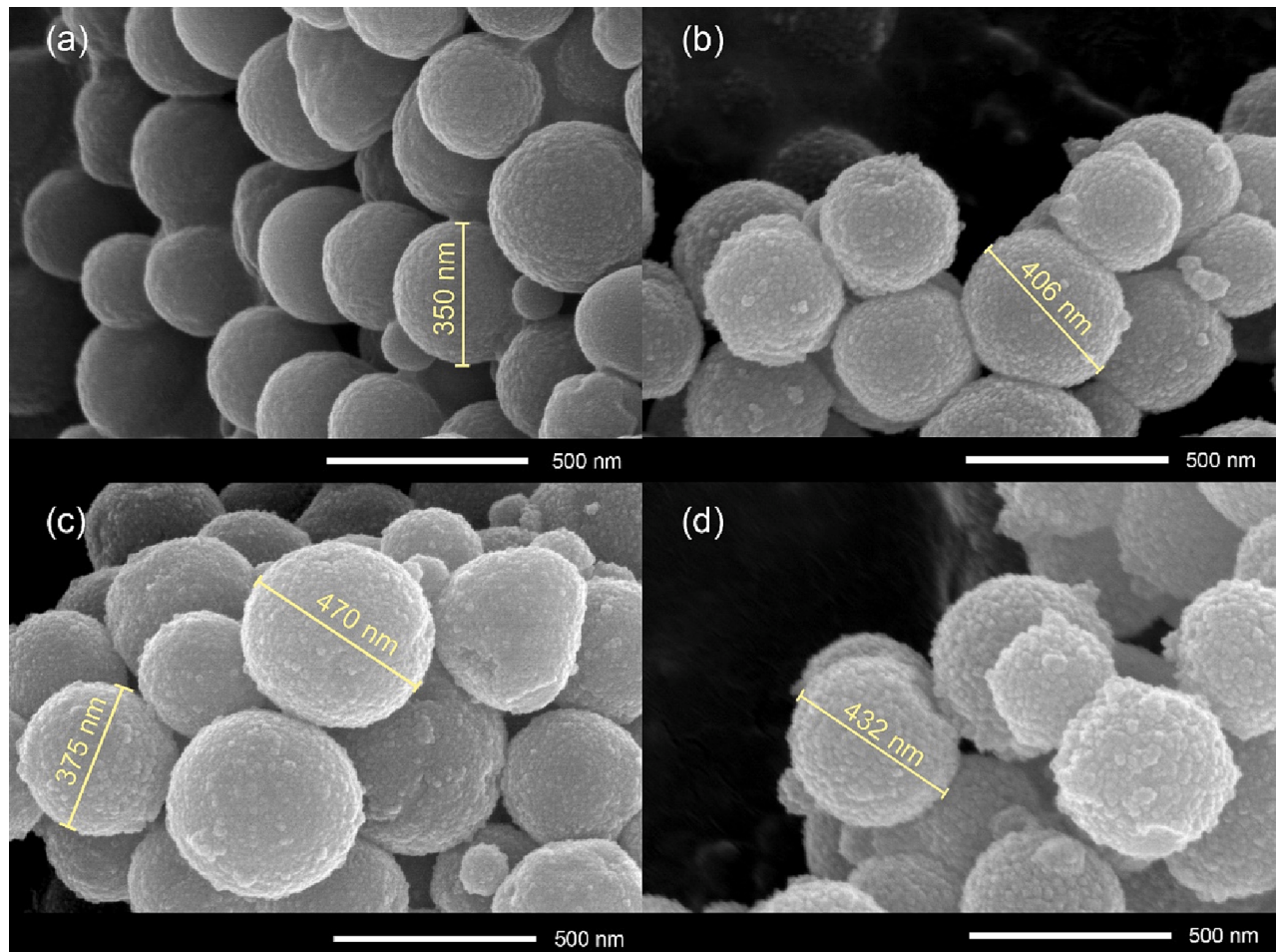


Fig. 1. SEM images of (a) PS, (b) PS@CeO₂, (c) PS@CeO₂:La, and (d) PS@CeO₂:Yb.

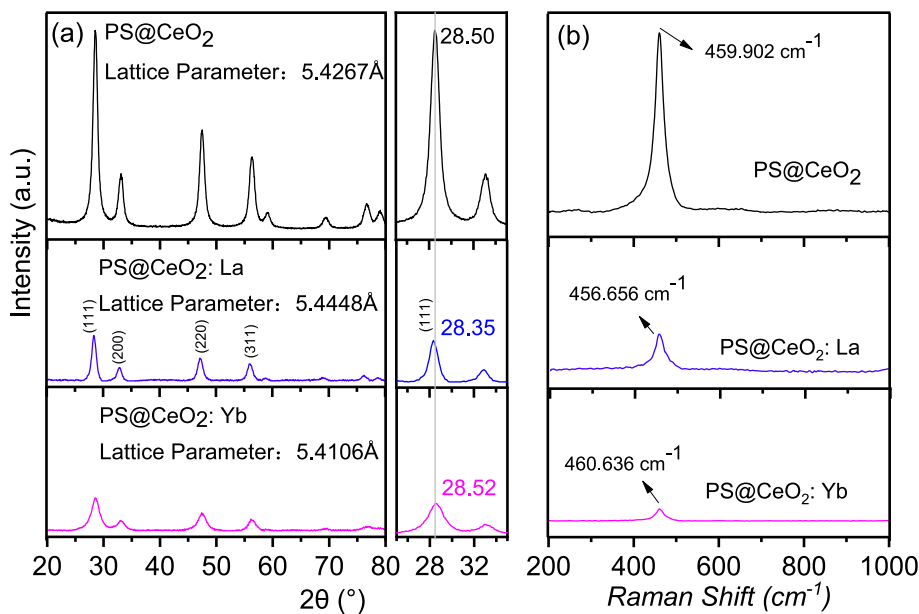


Fig. 2. (a) XRD patterns and a magnified view of the diffraction peak related to (111) plane for PS@CeO₂, PS@CeO₂:La, and PS@CeO₂:Yb. (b) Raman spectra of PS@CeO₂, PS@CeO₂:La, and PS@CeO₂:Yb.

Table 3

The lattice parameter (a), grain size (D), Raman peak, Ce³⁺ content, and CeO₂ shell proportion of the synthesized core–shell CeO₂-based abrasives.

Samples	a (Å)	D (nm)	Raman peak (cm ⁻¹)	Ce ³⁺ content	CeO ₂ shell proportion (wt.%)
PS@CeO ₂	5.4267	9.0	459.9	9.79%	47.86
PS@CeO ₂ : La	5.4448	8.2	456.656	28.14%	46.18
PS@CeO ₂ : Yb	5.4106	6.7	460.636	15.42%	46.42

98%), and hexamethylenetetramine (HMT, ≥98.0%) were purchased from Shanghai Chemical Reagent Co. (China). Styrene (St), Ce (NO₃)₃·6H₂O (purity 99.5%), La(NO₃)₃·6H₂O (99%), and Yb (NO₃)₃·5H₂O (99.99%) were purchased from MACKLIN Biochemical Technology Co. Except that St was treated with 5 wt% of aqueous NaOH solution to remove the inhibitor before use, other chemical reagents were used without further purification.

The commercial CeO₂ abrasive (C-CeO₂) was bought from Xuan-cheng Jingrui New Materials Co., Ltd. The CeO₂-based industrial polishing powder (G-CeO₂) and the soda lime glass substrates used for CMP experiments were provided by CNBM Bengbu Design and Research Institute for Glass Industry Co., Ltd. The porous polyurethane polishing pad was bought from Shenzhen Fangda Grinding Technology Co., Ltd.

2.2. Preparation

Core-shell abrasives were prepared using a two-step method. The negative-charged PS (-) nanospheres were synthesized by emulsifier-free emulsion polymerization under a nitrogen atmosphere: 10 g St and 0.32 g AA were dispersed in 150 ml water in a flask with continuous stirring and heated to 70 °C gradually. After holding for 30 min, 0.41 g KPS (dissolved in 30 ml water) was added to initiate polymerization and maintained at 70 °C for 7 h, then cooled to room temperature to stop polymerization.

In a typical synthesis of core–shell abrasives, 4 ml of the prepared PS colloids were dispersed into 200 ml water and separated homogeneously with a cell grinder for 10 min as the core precursor. 50 ml of 0.02 mol·L⁻¹ Ce (NO₃)₃·6H₂O aqueous solution for the pure CeO₂, or of 0.019 mol·L⁻¹

Ce (NO₃)₃·6H₂O and 0.88 mmol·L⁻¹ La(NO₃)₃·6H₂O/Yb(NO₃)₃·5H₂O aqueous solution for the doped CeO₂, was added as the shell precursor and stirred for 30 min, then 50 ml of 25 mmol·L⁻¹ HMT aqueous solution was added to initiate the precipitation. The homogeneous suspension was heated at 80 °C for 2 h under stirring, then cooled to room temperature and aged for 1 h. The obtained sediments were separated by centrifugation and washed with ethanol, then dried at 80°C in the air for 2 h. The samples were labeled as PS@CeO₂, PS@CeO₂:La, and PS@CeO₂:Yb for the pristine core–shell CeO₂, La-doped core–shell CeO₂, and Yb-doped core–shell CeO₂, respectively. Deionized water was used throughout the synthesis process.

2.3. Structural characterization

The morphology and microstructure were analyzed by scanning electron microscope (SEM, S-4800, Hitachi). The nano-particle size analyzer (Zeta, Zetasizer Nano-ZS, Marven) measured the average particle size. High-resolution transmission electron microscopy (HRTEM, JEMS-F200, JEOL) equipped with an energy dispersive spectroscopy (EDS) system was adopted to visualize the composite nanospheres' core–shell morphology, lattice information, and element distribution. Before the observation, the powder samples were dispersed in ethanol and dripped onto the carbon film. The phase information and lattice structure were measured by X-Ray diffraction (XRD, RIGAKU D/MAX 2550/PC, Rigaku) under the operation voltage of 40 kV, current of 40 mA, and Cu K α ($\lambda = 1.54178 \text{ \AA}$) as the radiation source. Raman spectra were collected at ambient conditions using a microscopic confocal Raman spectrometer (Raman, LABRAM HR Evolution, HORIBA Jobin Yvon) with a 633 nm laser as the excitation source. The doping element contents were measured using an inductively coupled plasma mass spectrometer (ICP-OES, 7800, Agilent Technologies Inc.). The X-ray photoelectron spectroscopy (XPS, AXIS SUPRA, Krato) was carried out with a dual Mg/Al anode (Power $\geq 500 \text{ W}$), and the C–C signal at 284.8 eV calibrated the measured binding energy before the peak fitting. The molar ratio of Ce³⁺/Ce⁴⁺ was calculated based on the deconvolution of Ce 3d spin-orbit doublet using XPSPEAK software. The thermogravimetric and differential thermal analyses were conducted under an air atmosphere from 30 to 800°C at a heating rate of 10°C·min⁻¹ using a thermal analyzer (TG-DTA, DSCQ1000, TA). The surface topography, average roughness (R_a) over scans of 5.0 μm × 5.0 μm area, and profile

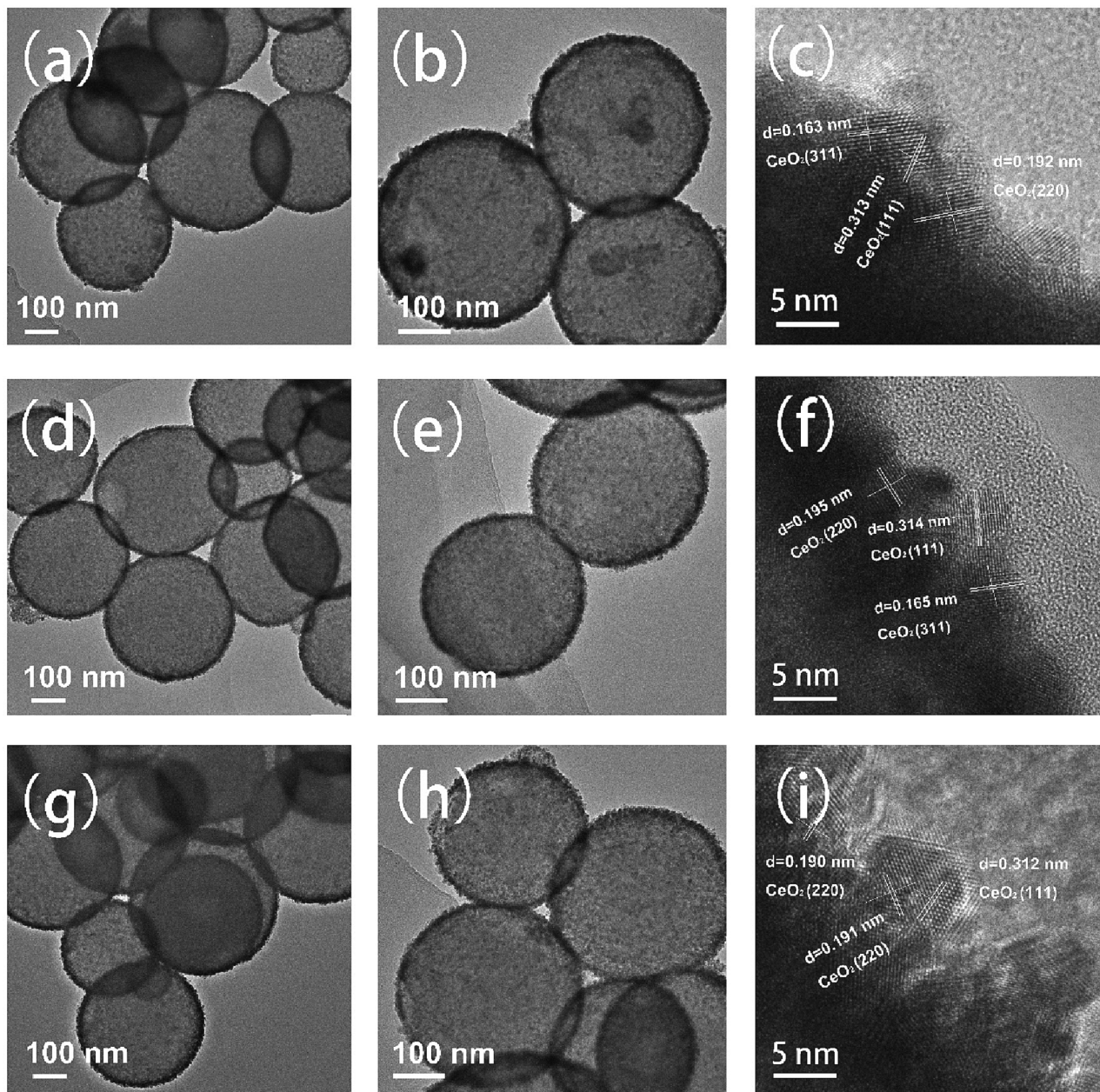


Fig. 3. TEM and HRTEM images of (a-c) PS@CeO₂, (d-f) PS@CeO₂:La, and (g-i) PS@CeO₂:Yb nanospheres.

curve were measured by atomic force microscope (AFM, Dimension ICON, Bruker) under the contact mode.

2.4. Polishing test

The soda lime glasses (20 mm × 20 mm × 2 mm) were used as the substrates and polished on a chemical mechanical polishing machine with a porous polyurethane pad (Alpha-600, Suzhou TROJAN Materials Technology Co.). After polishing, the substrates were rinsed sequentially with water and ethanol in an ultrasonic bath and then air-dried for the subsequent measurements. **Table 1** lists the polishing parameters.

The solid content was set at 1 wt% for the polishing slurry preparation, and the pH value was adjusted to 7 by 0.1 M NaOH aqueous solution. The polishing slurries were prepared based on PS@CeO₂, PS@CeO₂:La, and PS@CeO₂:Yb abrasives. The slurries based on C-CeO₂ and G-CeO₂ were designed as the control group. The weights of the glass substrate before and after polishing were measured by an electron

balance of exactly 0.01 mg (XS105, METTLER TOLEDO) to calculate the material removal rate (*MRR*) according to Eq. (1): [26]

$$MRR = \frac{\Delta m}{\rho s t} \quad (1)$$

where ρ is the density of the soda lime glass, equal to 2.52 g·cm⁻³ (Glass Density Measuring Instrument, MD-100, Beijing XuHui Xinrui Technology Co., Ltd.), s is the surface area, which is 4 cm² here, t is the polishing time, and Δm is the weight loss by polishing. Three parallel experiments were conducted for every polishing slurry, and the arithmetic mean values were used to present the *MRR* results.

3. Results and discussions

The quantitative element test was carried out by ICP-OES, as shown in **Table 2**. The measured doping concentrations of La and Yb are 4.41% and 4.43%, respectively, very close to the nominal value (4.4%),

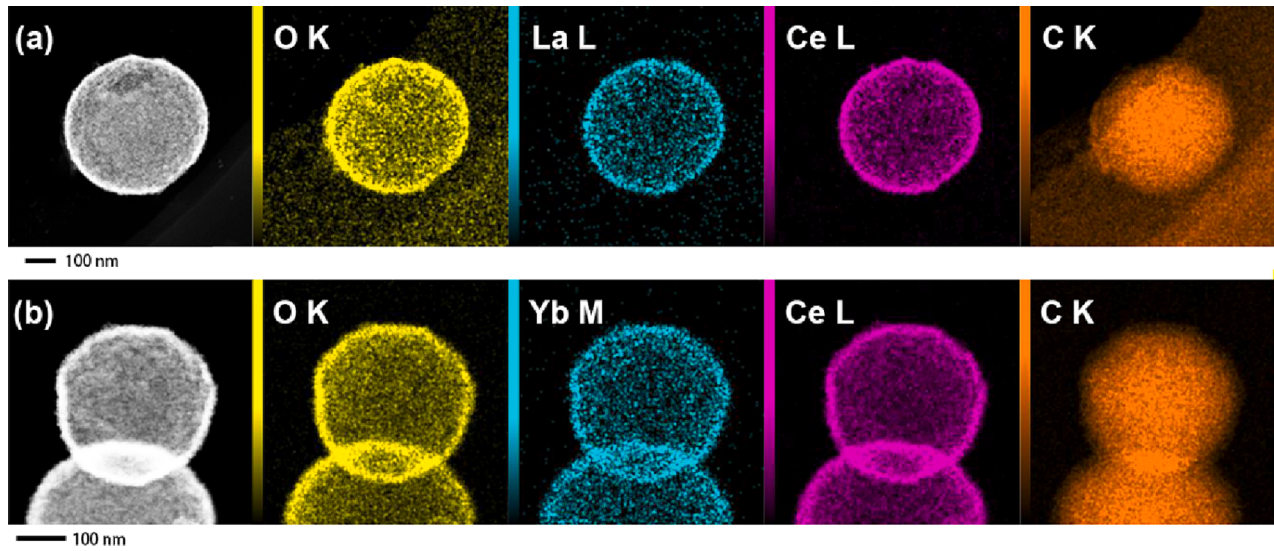


Fig. 4. Energy disperse spectroscopy (EDS) mapping images of the as-prepared nanospheres: (a) PS@CeO₂:La and (b) PS@CeO₂:Yb.

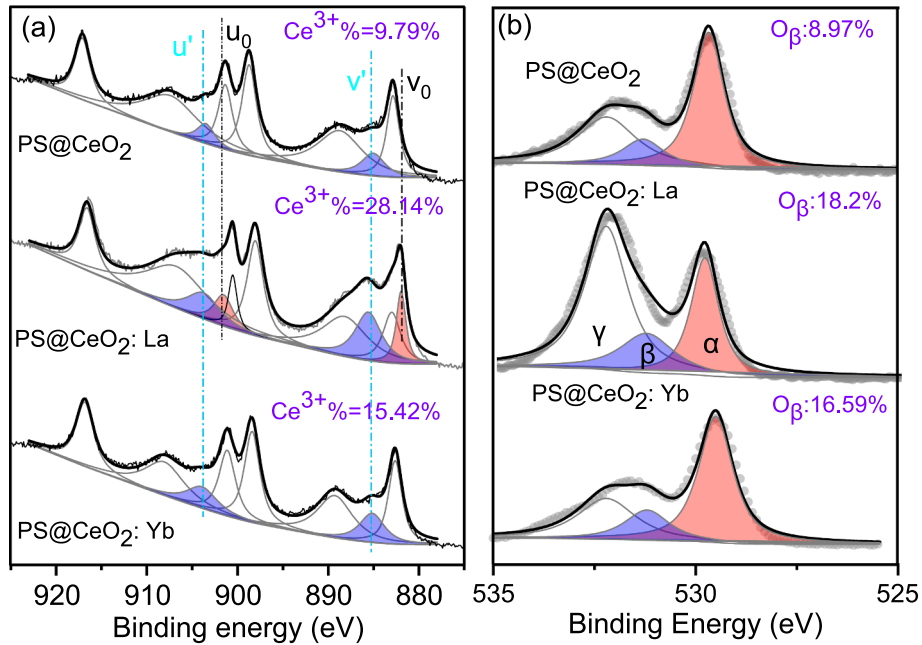


Fig. 5. XPS spectra of (a) Ce 3d and (b) O 1 s for PS@CeO₂, PS@CeO₂:La, and PS@CeO₂:Yb.

indicating that the precipitant method employed here can provide a reasonable dopant control. The morphological information of the PS core, PS@CeO₂, PS@CeO₂:La, and PS@CeO₂:Yb was tested by SEM, as shown in Fig. 1. The PS core exhibits a uniform spherical structure with a smooth surface. The average particle size is about 332 nm (Fig. 1a). Conversely, as illustrated in Fig. 1b ~ 1d, the outer surfaces of the three core-shell abrasives are composed of small nanocrystals, significantly rougher than that of the PS cores. The average particle sizes are about 377 nm, 381 nm, and 392 nm for PS@CeO₂, PS@CeO₂:La, and PS@CeO₂:Yb, respectively (see Fig. S1). The particle sizes were also measured using the dynamic light scattering method which confirmed the SEM statistical results, as listed in Table 2. Therefore, the calculated thickness of the CeO₂ shell is about 25 nm ~ 60 nm. Note that all core-shell particles exhibit a larger size than the reported abrasives [27–31], possibly leading to a higher material removal efficiency [13,32].

The XRD profiles of PS@CeO₂, PS@CeO₂:La, and PS@CeO₂:Yb are

shown in Fig. 2a. The diffraction peaks at about 28.5°, 33.0°, 47.4°, and 56.4° are respectively attributed to (111), (200), (220), and (311) crystal planes of fluorite CeO₂ (JCPDS NO. 43–1002) and no extra diffraction peaks related to La₂O₃ or Yb₂O₃ are found in the doped CeO₂, suggesting that the doping of La³⁺ or Yb³⁺ does not occasion the formation of the second phase. As shown in the magnified view of Fig. 2a, the diffraction peaks of the doped samples show a noticeable shift compared with the pristine CeO₂, preliminary suggesting that La³⁺ and Yb³⁺ are doped in the lattice. Moreover, for Yb³⁺ doping, the diffraction peaks shift significantly to the large angle direction ((111) plane, 28.50° → 28.52°), while for La³⁺ doping, the diffraction peaks shift to the small angle direction ((111) plane, 28.50° → 28.35°). Such tendency could be ascribed to the different ionic radii of Yb³⁺(0.97 Å) [33] and La³⁺(1.16 Å) [33–34], which are respectively smaller or larger than that of Ce⁴⁺ (0.97 Å) and Ce³⁺(1.07 Å) [35], resulting in the lattice shrinkage or expansion. The lattice parameters based on the XRD peaks are tabulated in Table 3, which are 5.4267 Å, 5.4448 Å, and 5.4106 Å for

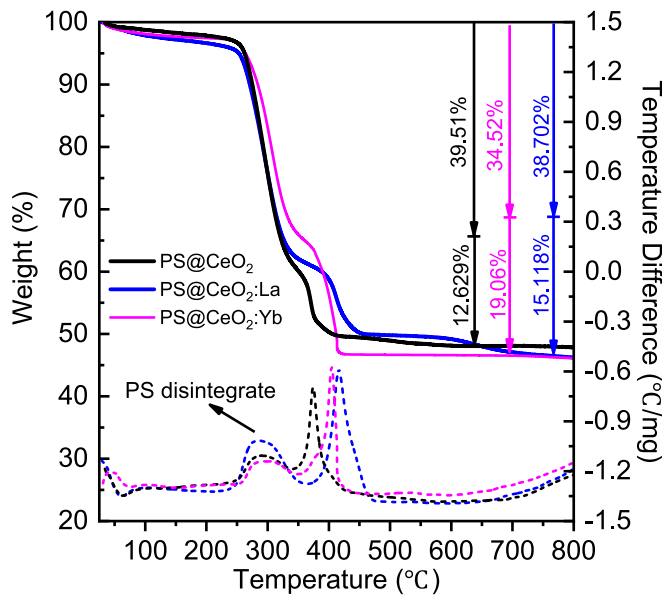


Fig. 6. TGA and DTA curves of the as-prepared core–shell abrasives.

PS@CeO₂, PS@CeO₂:La, and PS@CeO₂:Yb, respectively, further revealing the lattice distortion by the dopants. The grain sizes (D) were calculated by the Debye-Scherrer equation according to the (111) plane, as shown in Table 3, which are 9.0 nm, 8.2 nm, and 6.7 nm for PS@CeO₂, PS@CeO₂:La, and PS@CeO₂:Yb, respectively, indicating that the La³⁺ and Yb³⁺ dopings inhibit the crystalline of CeO₂. It is worth noting that the lattice distortion is not only affected by the radius mismatch between the La³⁺/Yb³⁺ and Ce ions but also related to the increased oxygen vacancies and Ce³⁺ concentration [34], which will be discussed later.

The Raman spectra are more indicative of the single-phase composition of the doped CeO₂ shells. As shown in Fig. 2b, only one peak is found near 460 cm⁻¹ in the range of 200 cm⁻¹–1000 cm⁻¹, assigned to the F_{2g} symmetric vibration mode of Ce-O-Ce. No other peaks corresponding to La₂O₃ or Yb₂O₃ [36] are found in the spectra. Additionally, a decrease in the wave number of the F_{2g} peak can be observed in the order of PS@CeO₂:Yb (460.636 cm⁻¹) > PS@CeO₂ (459.902 cm⁻¹) > PS@CeO₂:La (456.656 cm⁻¹). Such peak position shift is consistent with the lattice distortion raised by doping, confirming the preliminary conclusion suggested by XRD. For Yb³⁺ doped CeO₂, the lattice shrinkage results in a stronger bonding of Ce-O, causing a blue shift with a value of 3.256 cm⁻¹. In contrast, the doping of La³⁺ expands the CeO₂ lattice, leading to a red shift with a value of 0.734 cm⁻¹. Combining the analysis of Raman spectra and XRD diffraction, it can be concluded that the two-step method in this work successfully prepared the core–shell nanospheres with tiny doping of La³⁺/Yb³⁺ and that the dope caused microscopic lattice changes in the CeO₂ shell.

Based on the TEM images (Fig. 3), one can see an apparent contrast between the thin dark edge and large lighter center of all abrasives synthesized in this work, exhibiting well-defined core–shell structures. The average particle size information calculated from the TEM is 382.4 nm, 388.7 nm, and 389.1 nm for PS@CeO₂, PS@CeO₂:La, and PS@CeO₂:Yb, respectively, consistent with SEM and light scattering data. According to the HRTEM image of PS@CeO₂, the plane spacing of the shell particles was measured to be 0.313 nm, 0.192 nm, and 0.163 nm, corresponding to the (111), (220), and (311) plane spacing of pure CeO₂, respectively [37–38]. Meanwhile, the doped core–shell CeO₂ exhibits an increased/decreased plane spacing according to doping La³⁺/Yb³⁺, which is in harmony with the conclusion of XRD and Raman spectra.

The EDS mapping images of PS@CeO₂:La and PS@CeO₂:Yb are shown in Fig. 4, which directly demonstrate the organic core and CeO₂ shell structured nanospheres, simultaneously showing a homogeneous

distribution of the doped La³⁺/Yb³⁺, confirming no second phase generation, which is consistent with the above characterization analysis.

The high-resolution XPS spectra of Ce 3d are shown in Fig. 5a. The complex Ce 3d region can be fitted according to Romeo et al. [39] with ten components that take into account the spin-orbit split Ce 3d_{5/2}, Ce 3d_{3/2}, and other splitting caused by a redistribution of the entire energy spectrum after a core hole is created [37]. The content of Ce³⁺ can be calculated based on the area fraction of Ce³⁺ in the total area (Ce³⁺ and Ce⁴⁺), as shown in Table 3. As expected, the RE³⁺ doping increases the content of Ce³⁺. PS@CeO₂:La exhibits the highest concentration of Ce³⁺ (28.14%), which is two times greater than that of PS@CeO₂ (9.79%), while the Ce³⁺ enrichment of the Yb³⁺ doping is relatively low (15.42%).

The XPS spectra in the O 1 s region can be deconvoluted into three peaks, as shown in Fig. 5b, centered at about 527.8 eV, 531.3 eV, and 532.3 eV, which could be assigned to the O²⁻ ions in the CeO₂ lattice (denoted as O_a), the bound oxygen related to the presence of V_O in a matrix of CeO₂ (denoted as O_b), and the absorbed oxygen (denoted as O_c), respectively [40]. Based on the peak area ratio, the calculated content of O_b species show a decrease order of PS@CeO₂:La (O_b%=18.2%) > PS@CeO₂:Yb (O_b%=16.59%) > PS@CeO₂ (O_b%=8.97%), consistent with the tendency of the Ce³⁺ content, suggesting that La³⁺ exhibit stronger tunability of the chemical shift in CeO₂ than Yb³⁺. Since the lattice expansion caused by La³⁺ could compensate for the lattice shrinkage caused by oxygen vacancies, the system is easier to achieve stress equilibrium with La³⁺ doping, which is more inducible for forming oxygen defects, facilitating the reduction of Ce⁴⁺ to Ce³⁺ because of the charge balance. Thus, PS@CeO₂:La perform better enhancement on Ce³⁺ components in CeO₂ lattice than PS@CeO₂:Yb.

In addition, the XPS analysis of La³⁺/Yb³⁺ in PS@CeO₂:La and PS@CeO₂:Yb demonstrates the La³⁺-O/Yb³⁺-O formation [41–42] (see Fig. S2), which is consistent with the inferences drawn from XRD and Raman analysis.

The TG and DTA tests were carried out to quantitatively analyze the solid content of the core–shell abrasives, as shown in Fig. 6. Three weight loss stages could be found for all three samples. In the first stage, before 250 °C, a slight weight loss can be attributed to water's evaporation. In the second stage, up to about 410 °C, the sharp weight loss could be ascribed to the consecutive decomposition of the PS cores. The weight losses are about 39.51%, 38.70%, and 34.52% for PS@CeO₂, PS@CeO₂:La, and PS@CeO₂:Yb, respectively. Then in the third stage, up to about 700 °C, the weight losses are about 12.62%, 19.06%, and 15.12% for PS@CeO₂, PS@CeO₂:La, and PS@CeO₂:Yb, respectively. These sharper losses could be attributed to the oxidation of the residual polymers [38]. Since the residual weight comes from the CeO₂ shell, the weight ratios of CeO₂ in three core–shell abrasives calculated from TGA are about 47.86%, 46.18%, and 46.42% for PS@CeO₂, PS@CeO₂:La, and PS@CeO₂:Yb, respectively, simultaneously indicate that they have a similar core–shell structure, further proves the analysis conclusions of SEM and TEM. Therefore, the actual weight of CeO₂ used in the homemade polishing slurries will be 50% less than that of the commercially available slurries, matching the sustainability request in future CMP [43].

Before the CMP test, the surface morphology of the glass substrates was characterized by AFM, showing a relatively rough feature with irregular spherical projections, and the R_a value was 3.08 nm (see Fig. S3). The surface characteristics of the glass substrates after CMP with the synthesized core–shell abrasives were analyzed by AFM in three-dimensional (3D) and two-dimensional (2D) modes, as shown in Fig. 7. A few slight scratches were observed on the PS@CeO₂ polished glass substrate (Fig. 7a). In contrast, no scratch but some small protrusions on the PS@CeO₂:La and PS@CeO₂:Yb polished glass substrates are found (Fig. 7b and 7c). The line profiles along the diagonal in the 2D AFM images were also selected to facilitate the subsequent comparison and analysis. The corresponding results reveal the Max valley depth (R_v) of about 1.95 nm, 0.79 nm, and 1.57 nm for glasses polished by

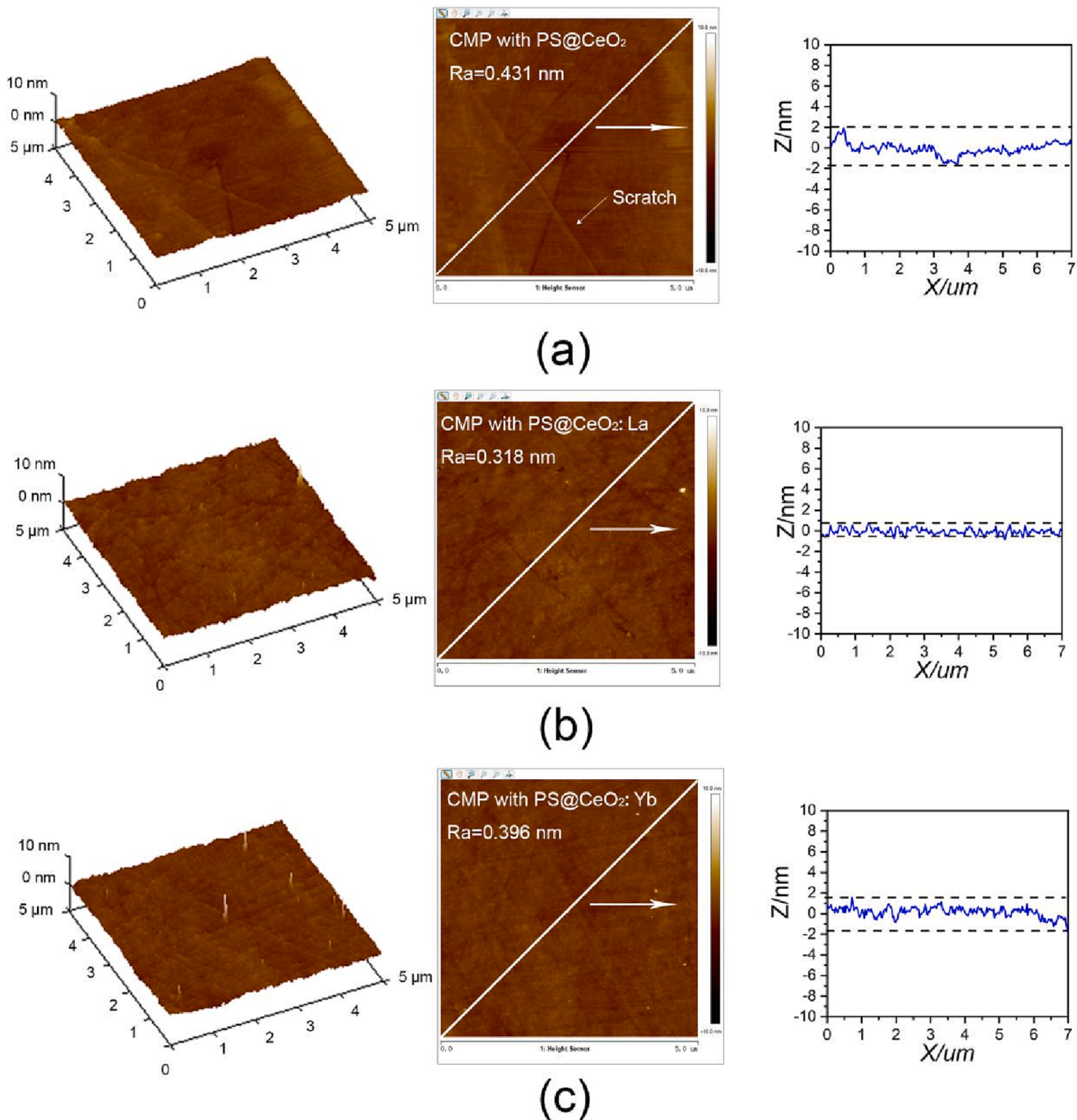


Fig. 7. 3D-, 2D-AFM images and profile curves of the glass substrates after CMP with (a) PS@CeO₂, (b) PS@CeO₂:La, and (c) PS@CeO₂:Yb.

Table 4
MRR, Ra, and Rv of the glass substrates after CMP with various abrasives.

Samples	PS@CeO ₂	PS@CeO ₂ : La	PS@CeO ₂ : Yb	C-CeO ₂	G-CeO ₂
MRR (nm/ min)	439.77 ± 17.79	480.22 ± 15.04	429.60 ± 17.88	338.00 ± 13.22	394.02 ± 19.44
Ra (nm)	0.43	0.32	0.40	1.33	0.57
Rv (nm)	1.95	0.79	1.57	5.48	3.18

PS@CeO₂, PS@CeO₂:La, and PS@CeO₂:Yb, respectively, indicating that PS@CeO₂:La exhibits the highest planarization ability.

The average MRR, Ra, and Rv values were summarized in [Table 4](#) and [Fig. 8](#) to evaluate the polishing performance quantitatively.

All core-shell abrasives synthesized here performed a higher material removal rate than the control group C-CeO₂ by about 27.09% – 42.07% (see [Fig. S4a](#)) and G-CeO₂ by about 9.03% – 21.88% (see [Fig. S4b](#)), confirming the superiority of core-shell structure, as discussed in the introduction section. Such improvement could be mainly attributed to their large particle size and the increased active CeO₂ caused by the PS core [13,32]. Meanwhile, core-shell abrasives exhibit excellent

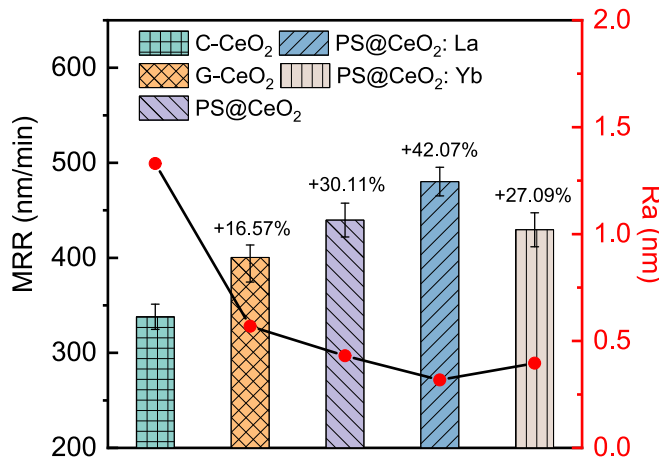


Fig. 8. CMP performance data of the various abrasives.

planar ability with Ra less than 0.5 nm, while for C-CeO₂ and G-CeO₂, the Ra values are 1.33 and 0.57, respectively. Such a phenomenon could be attributed to the lower elastic moduli induced by the PS core, according to the previous research conducted by Chen et al [16,19].

Among the core-shell abrasives, PS@CeO₂:La shows the highest polishing efficiency, which improves by 9.2% in MRR and reduces by 75.94% in Ra compared with PS@CeO₂. According to previous reports [24,44], the material removal ability of CeO₂ on glass is positively correlated to internal Ce³⁺ fraction, which will facilitate the frictional chemical activity between CeO₂-SiO₂, thereby improving the material removal efficiency. As discussed in the XPS results, PS@CeO₂:La has the highest Ce³⁺ concentration, leading to the best removal efficiency, supposing that Ce³⁺ plays a vital role in tearing down the SiO₂ hydrated layer. Meanwhile, the decreased crystallinity of PS@CeO₂:La and PS@CeO₂:Yb can reduce surface scratches to the glass, contributing to the precision of the polished glass, which is consistent with the Ra values calculated by AFM.

In summary, low-concentration doping of rare earth ions La³⁺ and Yb³⁺ effectively regulates Ce³⁺ components within CeO₂. It reduces the crystallinity of the CeO₂ shell, which significantly improves the polishing efficiency and increases the precision of the glass surface during CMP. The characterization and performance analysis of three core-shell samples confirmed the advantage of core-shell structures and further optimization of the core-shell abrasive system by doping modification, which compensates for the deficiency of research on PS@CeO₂ in the field of glass polishing and provides a brief reference for the selection of polishing parameters selection for glass CMP research.

4. Conclusion

The present work proposes a novel abrasive design scheme suitable for glass surface flattening, using a facile, low-temperature, controllable two-step method to prepare core-shell structured rare earth ion doping CeO₂, around 400 nm. TEM and EDS tests demonstrate the RE³⁺ doped CeO₂ outer shell and the inner PS core. The core-shell abrasives synthesized here exhibit an enhanced polishing efficiency of 27.09% – 42.07% and significantly better planarization ability than commercial CeO₂ due to the larger particle radius and spring-like effect introduced by the PS core. Among the core-shell abrasives, PS@CeO₂:La shows the highest material removal efficiency ($MRR = 480.22 \text{ nm/min}$) and the flattest polished surface ($Ra = 0.32 \text{ nm}$), which could be attributed to the highest concentration of Ce³⁺ resulting from the larger ionic radii of La³⁺. The results of the current work provide a strategy to optimize the abrasives and indicate that La-doped core-shell CeO₂ is an excellent abrasive for high-performance CMP.

CRediT authorship contribution statement

Zhuolun Li: Methodology, Validation, Data curation, Writing – original draft. Liangmao Jin: Validation. Zhiqiang Cao: Validation. Chong Zhang: Validation. Gaorong Han: Supervision. Shou Peng: Resources. Yong Liu: Writing – review & editing, Supervision.

Declaration of Competing Interest

The authors declare the following financial interests/personal relationships which may be considered as potential competing interests: [Yong Liu reports financial support was provided by Zhejiang University.]

Data availability

Data will be made available on request.

Acknowledgment

This work was supported by the 14th Five-Year National Key R&D Program [No. 2022YFB3603300 and No. 2021YFB3501100], the National Natural Science Foundation of China [U1809217], and the Opening Project of the State Key Laboratory of Advanced Technology for Float Glass.

Appendix A. Supplementary material

Supplementary data to this article can be found online at <https://doi.org/10.1016/j.apsusc.2023.158055>.

References

- [1] A. Plichta, A. Weber, A. Habeck, Ultra Thin Flexible Glass Substrates, MRS Online Proceedings Library (OPL) 769 (2003) H9.1.
- [2] D. Wang, J. Hauptmann, C. May, OLED Manufacturing on Flexible Substrates Towards Roll-to-Roll, MRS Adv. 4 (2019) 1367–1375.
- [3] F. Gao, C. Liu, L. Zhang, T. Liu, Z. Wang, Z. Song, H. Cai, Z. Fang, J. Chen, J. Wang, M. Han, J. Wang, K. Lin, R. Wang, M. Li, Q. Mei, X. Ma, S. Liang, G. Gou, N. Xue, Wearable and flexible electrochemical sensors for sweat analysis: a review, Microsyst. Nanoeng. 9 (2023) 1.
- [4] Y. Yalikun, Y. Hosokawa, T. Iino, Y. Tanaka, An all-glass 12 μm ultra-thin and flexible micro-fluidic chip fabricated by femtosecond laser processing, Lab Chip 16 (2016) 2427–2433.
- [5] M.-H. Ha, J.-K. Choi, B.-M. Park, K.-Y. Han, Highly flexible cover window using ultra-thin glass for foldable displays, J. Mech. Sci. Technol. 35 (2021) 661–668.
- [6] H. Aida, T. Doi, H. Takeda, H. Kataoka, S.-W. Kim, K. Koyama, T. Yamazaki, M. Uneda, Ultraprecision CMP for sapphire, GaN, and SiC for advanced optoelectronics materials, Curr. Appl. Phys. 12 (2012) S41–S46.
- [7] M. Tsujimura, The way to zeros: The future of semiconductor device and chemical mechanical polishing technologies, Jpn. J. Appl. Phys. 55 (2016) 06JA01.
- [8] S. A-C, Some Technical Aspects of Glass Substrates for TFT LCD Applications, Glass Technology - European Journal of Glass Science and Technology Part A. 44 (2003) 148–151.
- [9] R.K. Pal, H. Garg, V. Karar, Material removal characteristics of full aperture optical polishing process, Mach. Sci. Technol. 21 (2017) 493–525.
- [10] H. Cheng, Z. Dong, X. Ye, H.Y. Tam, Subsurface damages of fused silica developed during deterministic small tool polishing, Opt Express. 22 (2014) 18588–18603.
- [11] C.-C. Chen, H.-T. Young, C. Ching Hui, M.-Y. Xue, C.-L. Pan, Study on CMP process of glass wafers with SiO₂ based slurry for trench-glass-via interposer. 2016; p 1–6.
- [12] H. Lei, B.W. Naijing, Z. Zhang, C. Ruling, Chemical Mechanical Polishing of Glass Substrate with α-Alumina-g-Polystyrene Sulfonic Acid Composite Abrasive, Chinese Journal of Mechanical Engineering - CHIN J MECH ENG. 23 (2010).
- [13] M.-H. Oh, R.K. Singh, S. Gupta, S.-B. Cho, Polishing behaviors of single crystalline ceria abrasives on silicon dioxide and silicon nitride CMP, Microelectron. Eng. 87 (2010) 2633–2637.
- [14] T. Katoh, H.-G. Kang, U. Paik, J.-G. Park, Effects of Abrasive Morphology and Surfactant Concentration on Polishing Rate of Ceria Slurry, Jpn. J. Appl. Phys. 42 (2003) 1150.
- [15] Q. He, Experimental study on polishing performance of CeO₂ and nano-SiO₂ mixed abrasive, Applied. Nanoscience. 8 (2018) 163–171.
- [16] Y. Chen, W. Mu, J. Lu, Young's modulus of PS/CeO₂ composite with core/shell structure microspheres measured using atomic force microscopy, J. Nanopart. Res. 14 (2012).

- [17] Y. Chen, W.B. Mu, J.X. Lu, Determination of elastic modulus of composite PS/CeO₂ core-shell microspheres by atomic force microscope, *Mocaxue Xuebao/Tribology*. 32 (2012) 7–13.
- [18] Y. Chen, C. Qian, N. Miao, Atomic force microscopy indentation to determine mechanical property for polystyrene–silica core–shell hybrid particles with controlled shell thickness, *Thin Solid Films* 579 (2015) 57–63.
- [19] Y. Chen, Z. Li, N. Miao, Synergetic effect of organic cores and inorganic shells for core/shell structured composites abrasives for chemical mechanical planarization, *Appl. Surf. Sci.* 314 (2014) 180–187.
- [20] A. Chen, Z. Zhang, X. Li, Y. Chen, Evaluation of oxide chemical mechanical polishing performance of polystyrene coated ceria hybrid abrasives, *J. Mater. Sci. Mater. Electron.* 27 (2015) 2919–2925.
- [21] A. Chen, Y. Wang, J. Qin, Z. Li, Chemical Mechanical Polishing for SiO₂ Film Using Polystyrene@ceria (PS@CeO₂) Core–Shell Nanocomposites, *J. Inorg. Organomet. Polym Mater.* 25 (2015) 1407–1413.
- [22] L. M. J. J. O. N. C. S. Cook, Chemical processes in glass polishing, 120 (1990) 152–171.
- [23] K. Kim, D.K. Yi, U. Paik, Increase in Ce³⁺ Concentration of Ceria Nanoparticles for High Removal Rate of SiO₂ in Chemical Mechanical Planarization, *ECS J. Solid State Sci. Technol.* 6 (2017) P681.
- [24] J. Lee, E. Kim, C. Bae, H. Seok, J. Cho, K. Aydin, T. Kim, Improvement of oxide chemical mechanical polishing performance by increasing Ce³⁺/Ce⁴⁺ ratio in ceria slurry via hydrogen reduction, *Mater. Sci. Semicond. Process.* 159 (2023), 107349.
- [25] L. Wang, K. Zhang, Z. Song, S. Feng, Ceria concentration effect on chemical mechanical polishing of optical glass, *Appl. Surf. Sci.* 253 (2007) 4951–4954.
- [26] F.W. Preston, The Theory and Design of Plate Glass Polishing Machines, *J. Soc. Glas. Technol.* 11 (1927) 214–256.
- [27] A. Chen, J. Qin, Z. Li, Y. Chen, Engineering functionalized PS/mSiO₂ composite particles with controlled meso-shell thickness for chemical mechanical planarization applications, *J. Mater. Sci. Mater. Electron.* 28 (2016) 284–288.
- [28] Y. Chen, J. Qin, Y. Wang, Z. Li, Core/shell composites with polystyrene cores and meso-silica shells as abrasives for improved chemical mechanical polishing behavior, *J. Nanopart. Res.* 17 (2015).
- [29] Y. Chen, Y. Wang, J. Qin, A. Chen, Core/Shell Structured Solid-Silica/Mesoporous-Silica Microspheres as Novel Abrasives for Chemical Mechanical Polishing, *Tribol. Lett.* 58 (2015).
- [30] L. Zhang, H. Wang, Z. Zhang, F. Qin, W. Liu, Z. Song, Preparation of monodisperse polystyrene/silica core–shell nano-composite abrasive with controllable size and its chemical mechanical polishing performance on copper, *Appl. Surf. Sci.* 258 (2011) 1217–1224.
- [31] Y. Chen, R. Long, Polishing behavior of PS/CeO₂ hybrid microspheres with controlled shell thickness on silicon dioxide CMP, *Appl. Surf. Sci.* 257 (2011) 8679–8685.
- [32] A. Chen, Y. Chen, J. Ding, Polystyrene-Core Silica-Shell Composite Abrasives: The Influence of Core Size on Oxide Chemical Mechanical Planarization, *J. Electron. Mater.* 44 (2015) 2522–2528.
- [33] T. Hisashige, Y. Yamamura, T. Tsuji, Thermal expansion and Debye temperature of rare earth-doped ceria, *J. Alloy. Compd.* 408–412 (2006) 1153–1156.
- [34] F.J. Trindade, S. Damasceno, L. Otubo, M.R. Felez, D.Z. De Florio, F.C. Fonseca, A. S. Ferlauto, Tuning of Shape, Defects, and Disorder in Lanthanum-Doped Ceria Nanoparticles: Implications for High-Temperature Catalysis, *ACS Applied Nano Materials*, 5 (2022).
- [35] G. Li, Y. Zhao, Y. Wei, Y. Tian, Z. Quan, J. Lin, Novel yellowish-green light-emitting Ca₁₀(PO₄)₆O:Ce(3+) phosphor: structural refinement, preferential site occupancy and color tuning, *Chem. Commun.* 52 (2016) 3376–3379.
- [36] J. Cui, G.A. Hope, Raman and Fluorescence Spectroscopy of CeO₂, Er₂O₃, Nd₂O₃, Tm₂O₃, Yb₂O₃, La₂O₃, and Tb₄O₇, *J. Spectrosc.* 2015 (2015) 1–8.
- [37] F. Jiang, S. Wang, B. Liu, J. Liu, L. Wang, Y. Xiao, Y. Xu, X. Liu, Insights into the Influence of CeO₂ Crystal Facet on CO₂ Hydrogenation to Methanol over Pd/CeO₂ Catalysts, *ACS Catal.* 10 (2020) 11493–11509.
- [38] C. Zhou, X. Xu, L. Dai, H. Gong, S. Lin, Chemical-mechanical polishing performance of core-shell structured polystyrene@ceria/nanodiamond ternary abrasives on sapphire wafer, *Ceram. Int.* 47 (2021) 31691–31701.
- [39] M. Romeo, K. Bak, J.E. Fallah, F.L. Normand, L.J.S. Hilaire, I. Analysis, XPS Study of the reduction of cerium dioxide, 20 (1993) 508–512.
- [40] S. Sonsupap, A. Waehayee, T. Siritanon, W. Saenrang, N. Chanlek, H. Nakajima, A. Rattanachata, S. Maensiri, Structural, optical, and photocatalytic properties of La³⁺ doped CeO₂ nanospheres for enhanced photodegradation of tetracycline, *Colloids Surf. A Physicochem. Eng. Asp.* 659 (2023), 130650.
- [41] M.M. Natile, A. Galenda, A. Glisenti, From La₂O₃ To LaCoO₃: XPS Analysis, *Surf. Sci. Spectra* 15 (2010) 1–13.
- [42] Y. Wang, Z. Chen, P. Han, Y. Du, Z. Gu, X. Xu, G. Zheng, Single-Atomic Cu with Multiple Oxygen Vacancies on Ceria for Electrocatalytic CO₂ Reduction to CH₄, *ACS Catal.* 8 (2018) 7113–7119.
- [43] H. Lee, H. Kim, H. Jeong, Approaches to Sustainability in Chemical Mechanical Polishing (CMP): A Review, *Int. J. Precis. Eng. Manuf.-Green Technol.* 9 (2022) 349–367.
- [44] J. Ma, N. Xu, Y. Luo, Y. Lin, Y. Pu, Enhancing the Polishing Efficiency of CeO₂ Abrasives on the SiO₂ Substrates by Improving the Ce³⁺ Concentration on Their Surface, *ACS Appl. Electron. Mater.* 5 (2023) 526–536.